METHOD FOR RAPID INTERPLANETARY TRAJECTORY ANALYSIS USING ΔV MAPS WITH FLYBY OPTIONS

TAKUTO ISHIMATSU*, JEFFREY HOFFMAN†, AND OLIVIER DE WECK‡
Department of Aeronautics and Astronautics, Massachusetts Institute of Technology,
77 Massachusetts Avenue, Cambridge, MA 02139, USA.
Email: takuto@mit.edu*, jhoffma1@mit.edu†, deweck@mit.edu‡

This paper develops a convenient tool which is capable of calculating ballistic interplanetary trajectories with planetary flyby options to create exhaustive ΔV contour plots for both direct trajectories without flybys and flyby trajectories in a single chart. The contours of ΔV for a range of departure dates (x-axis) and times of flight (y-axis) serve as a "visual calendar" of launch windows, which are useful for the creation of a long-term transportation schedule for mission planning purposes. For planetary flybys, a simple powered flyby maneuver with a reasonably small velocity impulse at periapsis is allowed to expand the flyby mission windows. The procedure of creating a ΔV contour plot for direct trajectories is a straightforward full-factorial computation with two input variables of departure and arrival dates solving Lambert's problem for each combination. For flyby trajectories, a "pseudo full-factorial" computation is conducted by decomposing the problem into two separate full-factorial computations. Mars missions including Venus flyby opportunities are used to illustrate the application of this model for the 2020-2040 time frame. The "competitiveness" of launch windows is defined and determined for each launch opportunity.

Keywords: Interplanetary trajectory, C3, delta-V, pork-chop plot, launch window, Mars, Venus flyby

1. INTRODUCTION

The National Aeronautics and Space Administration's new plan for space exploration reaffirms that Mars is the ultimate goal of human exploration of the inner solar system [1-3]. It can be expected to see an increasing number of robotic explorations of Mars over the next several decades, eventually followed by human missions. In addition to determining the system architecture of such missions, the ability to design and analyze Mars transfer trajectories is an important planning tool. Planning future missions requires advance trajectory data such as departure and arrival dates (times of flight), C3, and ΔV for departure, arrival, and flyby maneuvers, if any.

The past studies of interplanetary trajectories have been mainly focused on launch windows on a window-by-window basis, creating a detailed C3 or ΔV contour plot (also known as a pork-chop plot) of one launch window or creating trajectory data tables that tabulate only one typical choice of departure and arrival dates for each launch window, which is selected based on a minimum C3 over the launch window. Assuming that future missions would be a long-term spaceflight campaign rather than individual missions, however, future mission designers should have more exhaustive in-hand trajectory data by which they can perform a trade-off analysis between C3 and time of flight within each launch window and even between neighboring launch windows. Thus, this paper focuses on creating exhaustive ΔV maps (extensive pork-chop plots) for both direct and flyby trajectories in a single chart, which, in the case of Mars missions, correspond to Earth-Mars trajectories (Fig. 1) and Earth-Venus-Mars trajectories (Fig. 2), respectively. In other words, while in the past studies pork-chop plots abound separately and flyby trajectories have also been analyzed in detail, this paper attempts to put direct and flyby flight opportunities together in a comprehensive ΔV map, allowing a preliminary assessment by mission architects as to what options

are available. The ΔV maps for an extensive range of departure dates (x-axis) and times of flight (y-axis) serve as a "visual calendar" of launch windows, which are useful for the creation of a long-term transportation schedule for mission planning purposes. Since this paper puts emphasis on launch-window expansion, deep space maneuvers (DSMs) such as broken plane maneuvers are not considered. It is known that those maneuvers could improve trajectory performance from an energetic point of view, but they do not make much difference in launch periods while flyby trajectories could open up totally new launch opportunities because the third planet is involved.

One of the important characteristics representing a trajectory is the energy required for departure, which is referred to as C3 ($= V_\infty^2$)[1]. A lower C3 is desired since it means a smaller velocity change for transfer injection, which consumes less fuel. A C3 for arrival also needs to be defined. A lower C3 for arrival also results in less fuel for braking or imposes a less stringent requirement for aerocapture. In this paper, for distinction, let $C3_d$ and $C3_a$ be the characteristic energies required for departure and arrival, respectively.

Planetary flybys are typically intended to save fuel by taking advantage of a planet's gravity to alter the path and speed of a spacecraft. Sticking to free flybys only, however, would narrow launch windows. Instead, if a small burn is allowed at flyby, it would be able to expand the flyby mission window. Therefore in this study, a simple powered flyby maneuver with a reasonably small velocity impulse at periapsis is allowed. In the case study of Mars missions described later, a velocity impulse of 0.3 [km/s] is selected as a "reasonable" upper bound for a powered flyby maneuver at periapsis, which is less than 10% of a typical ΔV required for departure from Earth.

To begin with, a trajectory calculation program is developed that solves Lambert's problem to determine a single orbit from a specified transfer time and two position vectors. Once a unique orbit is determined, C3 and ΔV are calculated. By repetition for a series of departure and arrival dates, the procedure of creating a ΔV contour plot for direct trajectories is straightforward.

On the other hand, since a flyby trajectory must specify three dates for departure, flyby encounter, and arrival, it is obvious that a full-factorial computation requires a large computational effort. However, considering the nature of Lambert's problem, the pre-flyby and post-flyby trajectories can be determined independently. A "pseudo full-factorial" computation procedure is formulated by decomposing the problem into two separate full-factorial computations [4-6]. The trajectory data for direct missions obtained by a full-factorial computation and for flyby missions obtained by a "pseudo full-factorial" computation can be put together in a single chart. Subsequently, a "bat chart" depicting flight opportunities is also drawn.

For a case study to illustrate the application of this model, Mars missions including Venus flyby opportunities are analyzed in the time frame 2020 to 2040, during which such missions seem most relevant. The competitiveness of Earth-Venus-Mars flyby trajectory windows with Earth-Mars direct trajectory windows is discussed.

[1] Derives its name from the third of three constants that Forest Ray Moulton (1872-1952) employed in presenting two-body motion in his influential textbook titled *An Introduction to Celestial Mechanics* (1914)

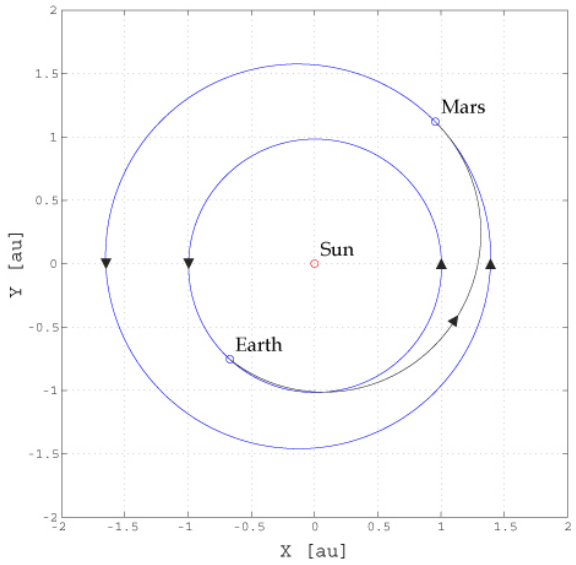

Fig. 1 Earth-Mars direct trajectory.

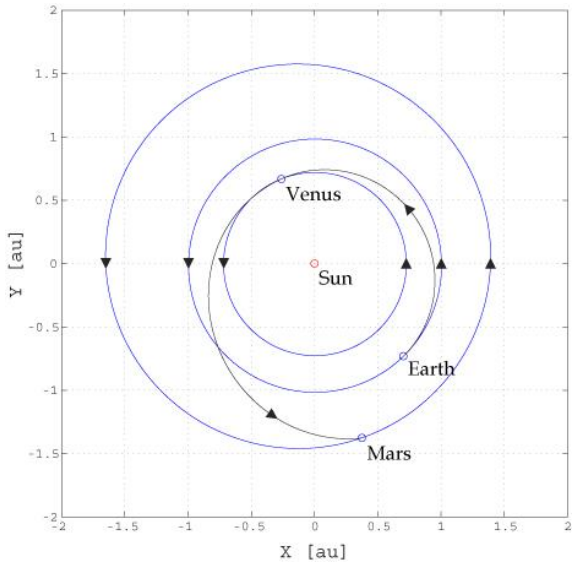

Fig. 2 Earth-Venus-Mars flyby trajectory.

2. DIRECT TRAJECTORY DATA

First a tool is developed that is capable of calculating a ballistic interplanetary trajectory given a transfer time an two position vectors. The code is validated by comparison with the data from Jet Propulsion Laboratory [7]. Once a unique orbit is determined, C3 and ΔV can be calculated. Then a full-factorial computation approach is formulated to obtain a ΔV contour plot for the time frame of interest.

2.1 Model for Solving Lambert's Problem

To determine an orbit from a specified transfer time and two position vectors, Lambert's problem needs to be solved. Over the years a variety of techniques for solving Lambert's problem have been developed [8]. In order to solve Lambert's problem in a more general way that is valid for all types of orbits, a universal variable is introduced in the Lagrange coefficients [9].

For consistency between direct and flyby trajectories, let the '1' and '3' subscripts represent the departure and arrival, respectively, and if any, let the '2' subscript represent the single flyby encounter. The mission of a direct trajectory is to send a spacecraft directly from planet 1 to planet 3 in a specified time between the departure and arrival dates. The flow chart in Fig. 3 shows the overall structure of this procedure.

Algorithm

Given planet 1, planet 3, and the departure and arrival dates, determine a direct trajectory from planet 1 to planet 3 and $C3_d$ and $C3_a$ in the following procedure: ①calculate the time of flight, TOF, using the Julian day numbering system (e.g. JD2458850.0 = 1/1/2011, 12:00PM), ②calculate planetary ephemeris to determine the state vector $\mathbf{r}_1$ and $\mathbf{v}_1$ of planet 1 at departure and the state vector $\mathbf{r}_3$ and $\mathbf{v}_3$ of planet 3 at arrival, ③determine the position vectors of spacecraft at departure and arrival, $\mathbf{r}_d$ and $\mathbf{r}_a$, by copying $\mathbf{r}_1$ and $\mathbf{r}_3$, respectively, ④use $\mathbf{r}_d$, $\mathbf{r}_a$, and TOF in solving Lambert's problem to find a spacecraft's velocity $\mathbf{v}_d$ at departure from planet 1 and its velocity $\mathbf{v}_a$ at arrival to planet 3, and ⑤calculate $C3_d$ ($= V_{\infty d}^2 = |\mathbf{v}_d - \mathbf{v}_1|^2$) and $C3_a$ ($= V_{\infty a}^2 = |\mathbf{v}_a - \mathbf{v}_3|^2$).

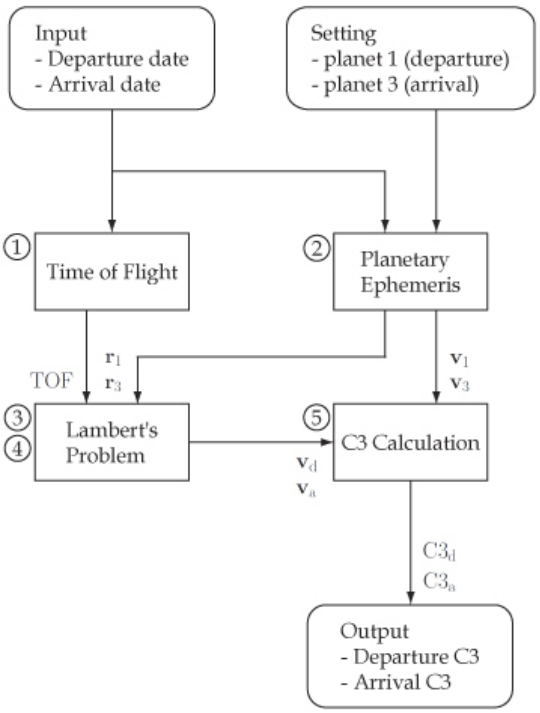

Fig. 3 Flow chart of calculating a single direct trajectory.

2.2 Full-Factorial Computation

The procedure of creating direct trajectory data is straightforward as seen in Fig. 4: it is a full-factorial computation just by wrapping Fig. 3 in doubly-nested "`for`" loops for a series of departure and arrival dates. The trajectory calculation in Fig. 3 is repeated over a range of t_1 and t_3 while satisfying $t_1 < t_3$.

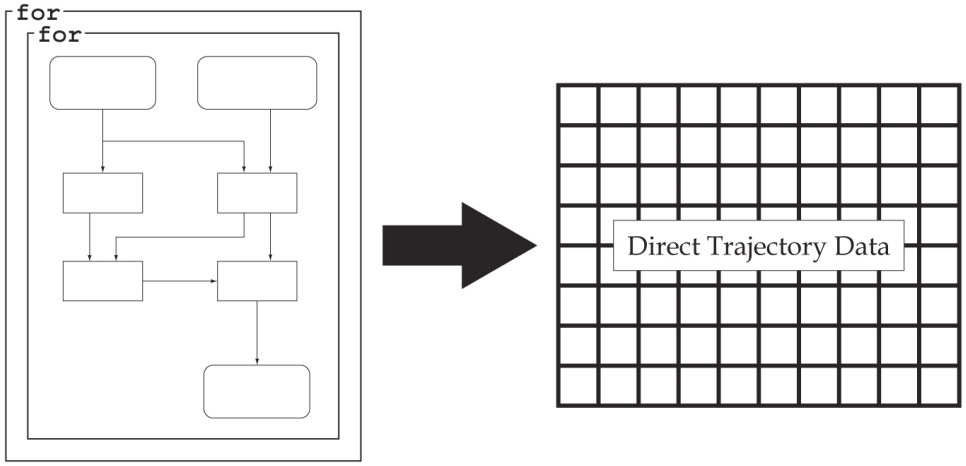

Fig. 4 Flow chart of a full-factorial approach to produce direct trajectory data.

3. FLYBY TRAJECTORY DATA

For flyby trajectory problems with three input variables instead of two, where an additional variable is the flyby encounter dates, it is obvious that a full-factorial computation will require a large computational effort. In this case study for 2020-2040 Mars missions, in which the range is 7500 days in the x-axis (departure date) and 700 days in the y-axis (time of flight) with a step of 2 days in both x and y directions, a full-factorial computation for direct

trajectories requires about 70 hours while that for flyby trajectories requires more than 36000 hours (MATLAB® used on Intel® Core™2 Duo processor at 2.40 GHz). Thus, a "pseudo full-factorial" approach is conducted by decomposing the problem into two separate full-factorial computations.

3.1 Powered Flyby Maneuver

Planetary flybys are typically intended to save fuel by taking advantage of a planet's gravity to alter the path and speed of a spacecraft. Sticking to free flybys only, however, would narrow launch windows. Instead, if a small burn is made at flyby, it would be able to expand the flyby mission windows. Therefore in this study, a simple powered maneuver with a reasonably small velocity impulse at periapsis is allowed.

Fig. 5 shows a hyperbolic flyby trajectory with a velocity increment at periapsis. Inbound and outbound hyperbolic excess velocity vectors relative to the flyby planet can, respectively, be expressed as:

$$\mathbf{V}_{\infty \mathrm{i}} = \mathbf{v}_{\mathrm{i}} - \mathbf{v}_{\mathrm{P}} \tag{1}$$

$$\mathbf{V}_{\infty \mathrm{o}} = \mathbf{v}_{\mathrm{o}} - \mathbf{v}_{\mathrm{P}} \tag{2}$$

where $\mathbf{v}_{\mathrm{i}}$ and $\mathbf{v}_{\mathrm{o}}$ are, respectively, the inbound and outbound velocity vectors of the spacecraft in the heliocentric frame and $\mathbf{v}_{\mathrm{P}}$ is the heliocentric velocity vector of the flyby planet. As illustrated in Fig. 5, let the '$-$' and '$+$' subscripts represent the pre-periapsis and post-periapsis trajectories, respectively. Thus, the total turn angle, $\nu_- + \nu_+$, must satisfy

$$\sin(\nu_- + \nu_+) = |\mathbf{V}_{\infty \mathrm{o}} \times \mathbf{V}_{\infty \mathrm{i}}| / V_{\infty \mathrm{o}} V_{\infty \mathrm{i}} \tag{3}$$

Since the pre-periapsis and post-periapsis trajectories intersect at periapsis with a radius of $\mathbf{r}_{\mathrm{m}}$, then

$$r_m = \mu_{\mathrm{P}} (\csc \nu_- - 1) / V_{\infty \mathrm{i}}^2 \tag{4}$$

$$r_m = \mu_{\mathrm{P}} (\csc \nu_+ - 1) / V_{\infty \mathrm{o}}^2 \tag{5}$$

so that

$$\sin \nu_- = 1 / \left(1 + V_{\infty \mathrm{i}}^2 / V_{\odot \mathrm{m}}^2\right) \tag{6}$$

$$\sin \nu_+ = 1 / \left(1 + V_{\infty \mathrm{o}}^2 / V_{\odot \mathrm{m}}^2\right) \tag{7}$$

where μ_{P} is the standard gravitational parameter of the planet and $V_{\odot \mathrm{m}}$ is a circular speed at radius r_{m}

$$V_{\odot \mathrm{m}}^2 = \mu_{\mathrm{P}} / r_{\mathrm{m}} \tag{8}$$

From Eqs. (3), (6), and (7), an implicit equation for r_{m} is obtained as:

$$\sin^{-1}\{|\mathbf{V}_{\infty \mathrm{o}} \times \mathbf{V}_{\infty \mathrm{i}}| / V_{\infty \mathrm{o}} V_{\infty \mathrm{i}}\} = \sin^{-1}\left\{1 / \left(1 + V_{\infty \mathrm{i}}^2 / V_{\odot \mathrm{m}}^2\right)\right\} + \sin^{-1}\left\{1 / \left(1 + V_{\infty \mathrm{o}}^2 / V_{\odot \mathrm{m}}^2\right)\right\} \tag{9}$$

In the above equation, the only unknown parameter is r_{m} through $V_{\odot \mathrm{m}}$. Therefore, this equation can be iteratively solved to determine r_{m}. If this r_{m} turns out to be smaller than the planet's radius, the spacecraft will crash into the surface. In order for the flyby to be feasible, the spacecraft must pass well above the surface, which requires that r_{m} be larger than the planet's radius plus the thickness of the atmosphere.

Once r_{m} is determined, the velocity of the spacecraft at periapsis on the pre- and post-periapsis trajectories, $V_{\mathrm{m}-}$ and $V_{\mathrm{m}+}$, can be computed in the following equations.

$$V_{\mathrm{m}-} = \sqrt{V_{\infty \mathrm{i}}^2 + 2\mu_{\mathrm{P}} / r_{\mathrm{m}}} \tag{10}$$

$$V_{m+} = \sqrt{V_{\infty o}^2 + 2\mu_P / r_m} \tag{11}$$

The difference between the above two equations is the change in velocity required for a powered flyby maneuver at periapsis:

$$\Delta V_{PFM} = V_{m+} - V_{m-} = \sqrt{V_{\infty o}^2 + 2\mu_P / r_m} - \sqrt{V_{\infty i}^2 + 2\mu_P / r_m} \tag{12}$$

which is positive when accelerating and negative when decelerating. A free flyby corresponds to $\Delta V_{PFM} = 0$ since $V_{\infty i} = V_{\infty o}$. Ideally, ΔV_{PFM} should be zero so that the spacecraft would not need to consume any fuel. But it would be worthwhile to look into the possibility of powered flyby, since allowing a small amount of ΔV_{PFM} might provide a much broader mission window.

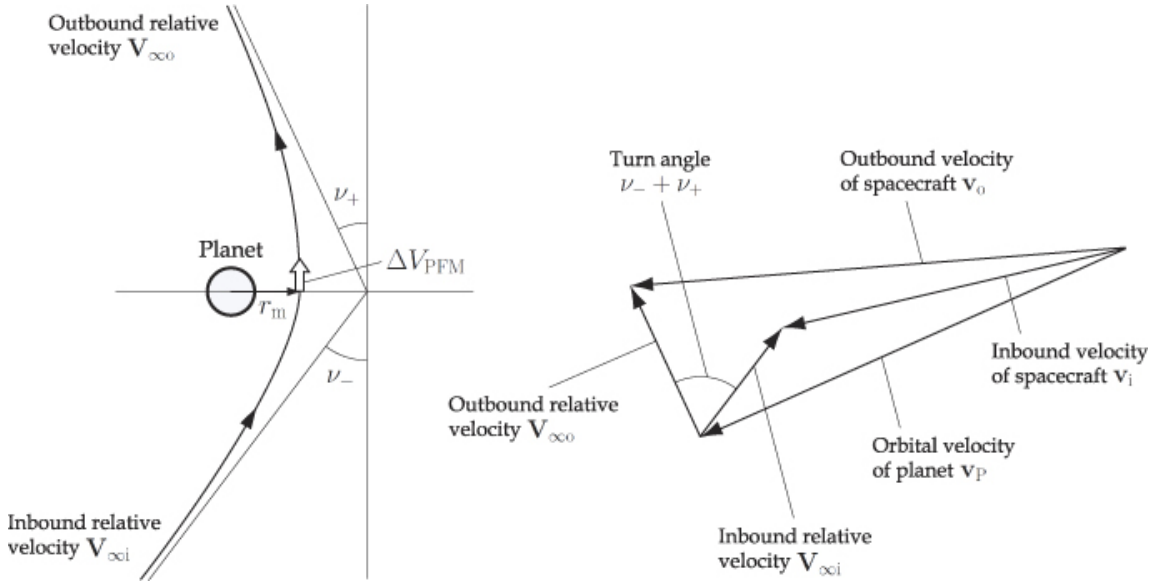

Fig. 5 Powered flyby maneuver with a velocity impulse of ΔV_{PFM} at periapsis.

3.2 Full-Factorial Computation

Before stepping into a "pseudo full-factorial" computation, the formulation of a full-factorial approach in a similar manner to the direct trajectory case is attempted. Fig. 6 shows the flow chart of calculating a single flyby trajectory for a specified set of three dates: departure, flyby encounter, and arrival. Thus the inputs are t_1, t_2, and t_3 while in the direct trajectory case the inputs are t_1 and t_3. The difference from Fig. 3 is that two Lambert's problems have to be solved for the trajectories from planet 1 to planet 2 and from planet 2 to planet 3. A flyby calculation shown in the previous section also needs to be performed as an interface between the two trajectories. At the end of this procedure, $C3_d$ and $C3_a$ are obtained as well as ΔV_{PFM} and a minimum passing altitude, h_m $(= r_m - r_P)$, which determines the flyby feasibility.

As shown in Fig. 7, the simplest way would be to wrap Fig. 6 in triple "`for`" loops for departure, flyby encounter, and arrival dates. In this way the trajectory calculation in Fig. 6 is repeated over a range of t_1, t_2, and t_3 while satisfying $t_1 < t_2 < t_3$. This is a "brute force" full-factorial computation. Compared to Fig. 3, there is an additional dimension in the input variables.

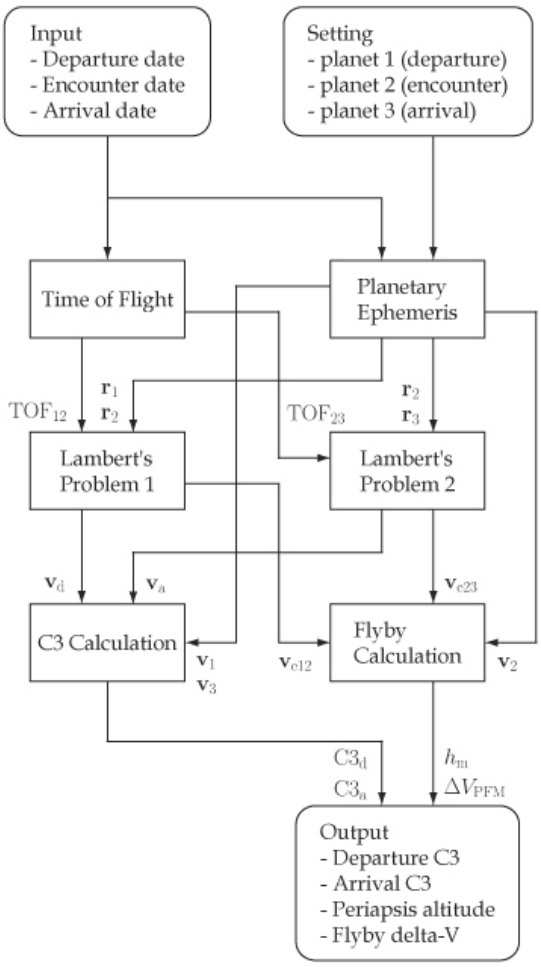

Fig. 6 Flow chart of calculating a single flyby trajectory.

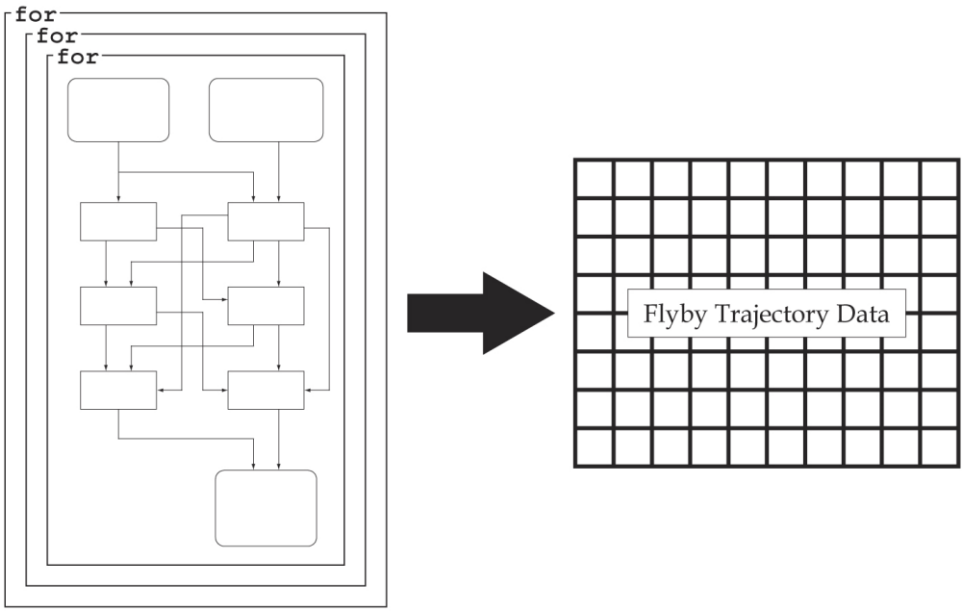

Fig. 7 Flow chart of a full-factorial approach to produce flyby trajectory data.

3.3 Pseudo Full-Factorial Computation

When trying to do a computation with a broad range of TOF or with a fine resolution, it can be imagined that this additional input variable will require much more computational effort. But, indeed, this procedure repeats the same calculations many times; after solving a flyby trajectory for specific t_1, t_2, and t_3, for example, when solving for t_1, t_2, and $t_3 + 1$, the same Lambert's problem for the combination of t_1 and t_2 is solved. This duplicated computation occurs hundreds of times, which wastes a lot of time.

Instead of such a straightforward approach, it should be noted that the pre-flyby and post-flyby trajectories can determined independently. A planetary flyby at t_2 is only an interface between the two trajectories since what is needed for the flyby calculation are $\mathbf{v}_{e12}$ and $\mathbf{v}_{e23}$. Therefore, full-factorial computations can be performed in advance for these two problems separately and the data can be stored in memory cache. By doing this beforehand, the memory cache can be accessed to obtain the information of these velocity vectors, $\mathbf{v}_{e12}$ and $\mathbf{v}_{e23}$, when the flyby calculations are performed later on. This process should be wrapped in triple "`for`" loops rather than Fig. 6 since in each repetition step, just accessing the memory cache takes much shorter time than solving an iterative Lambert's problem. By scanning t_2 for given t_1 and t_3, an optimal t_2 can be picked that will minimize ΔV for the combination of t_1 and t_3 while satisfying the mission feasibility. Fig. 8 shows the overall procedure of this "pseudo full-factorial" computation.

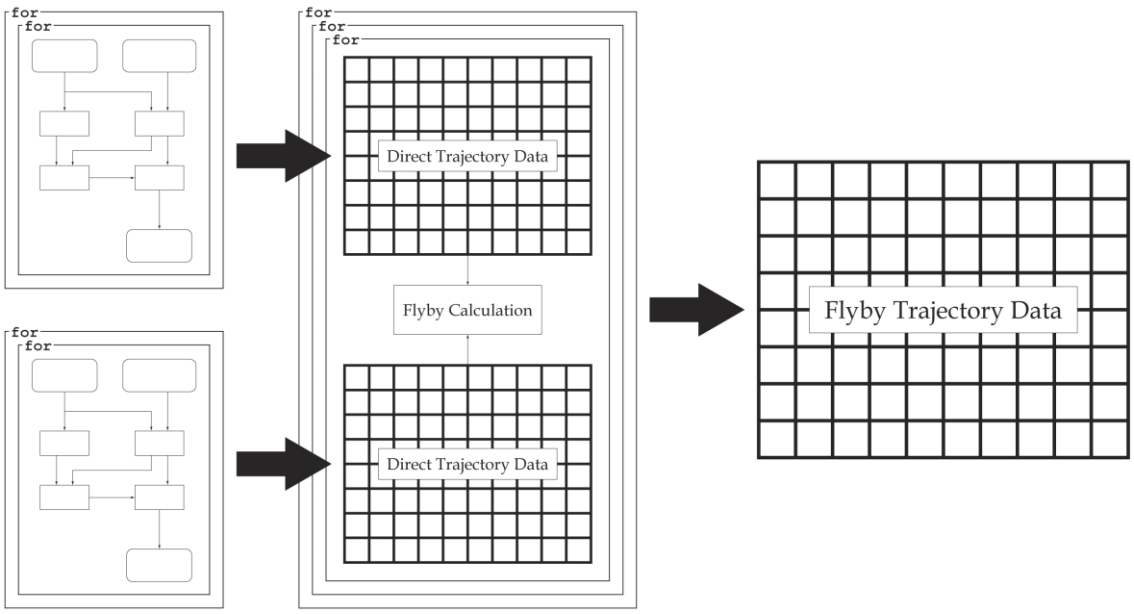

Fig. 8 Flow chart of a "pseudo full-factorial" approach to produce flyby trajectory data.

4. TRAJECTORY DATA ANALYSIS

Having formulated the method to obtain the exhaustive trajectory data for both direct and flyby cases, they are put together into a single chart to create a complete "launch window calendar." Subsequently, a "bat chart" depicting flight opportunities are drawn.

4.1 Integrated ΔV_{tot} Contours

Since two sets of trajectory data for direct and flyby have been obtained on the same range in the t_1-t_3 plane, selecting a superior one of the two trajectories at each point on the grid gives a direct/flyby integrated contour plot. If $C3_{\mathrm{d}}$ is used for the contour plot, however, it might be unfair since a flyby trajectory also requires ΔV_{PFM} for powered flyby maneuver. Instead, by converting $C3_{\mathrm{d}}$ into ΔV_{d} (ΔV required for departure), ΔV for departure and

powered flyby can be uniformly treated. Thus, if ΔV_{a} is ignored assuming aerocapture at arrival, ΔV_{tot} can be defined as:

$$\Delta V_{\mathrm{tot}} = |\Delta V_{\mathrm{d}}| + |\Delta V_{\mathrm{PFM}}| \tag{13}$$

which can be used for integration instead of $C3_{\mathrm{d}}$. In conversion from $C3_{\mathrm{d}}$ to ΔV_{d}, a departure hyperbola starting from a circular parking orbit with an altitude of h_{po} is assumed. The departure hyperbola has a periapsis radius equal to the radius of the parking orbit. If r_{po} is the radius of the parking orbit, the velocity required at the injection point is

$$V_{\mathrm{d}} = \sqrt{C3_{\mathrm{d}} + 2\mu_{\mathrm{P}}/r_{\mathrm{po}}} \tag{14}$$

Therefore, the ΔV required for departure is

$$\Delta V_{\mathrm{d}} = V_{\mathrm{d}} - V_{\mathrm{po}} = \sqrt{C3_{\mathrm{d}} + 2\mu_{\mathrm{P}}/r_{\mathrm{po}}} - \sqrt{\mu_{\mathrm{P}}/r_{\mathrm{po}}} \tag{15}$$

where V_{po} is a circular speed at radius r_{po}.

Fig. 9 shows an example of a direct/flyby integrated ΔV_{tot} contour plot. Note that each datatip in the figure shows the local minimum ΔV_{tot} for that part of the pork-chop plot. Since the x-axis represents departure date and the y-axis represents TOF, each 45° diagonal line represents a specific arrival date. Therefore, when looking at some point in the figure, one can find the departure date from right below as well as the arrival date by looking down along the arrival-date line.

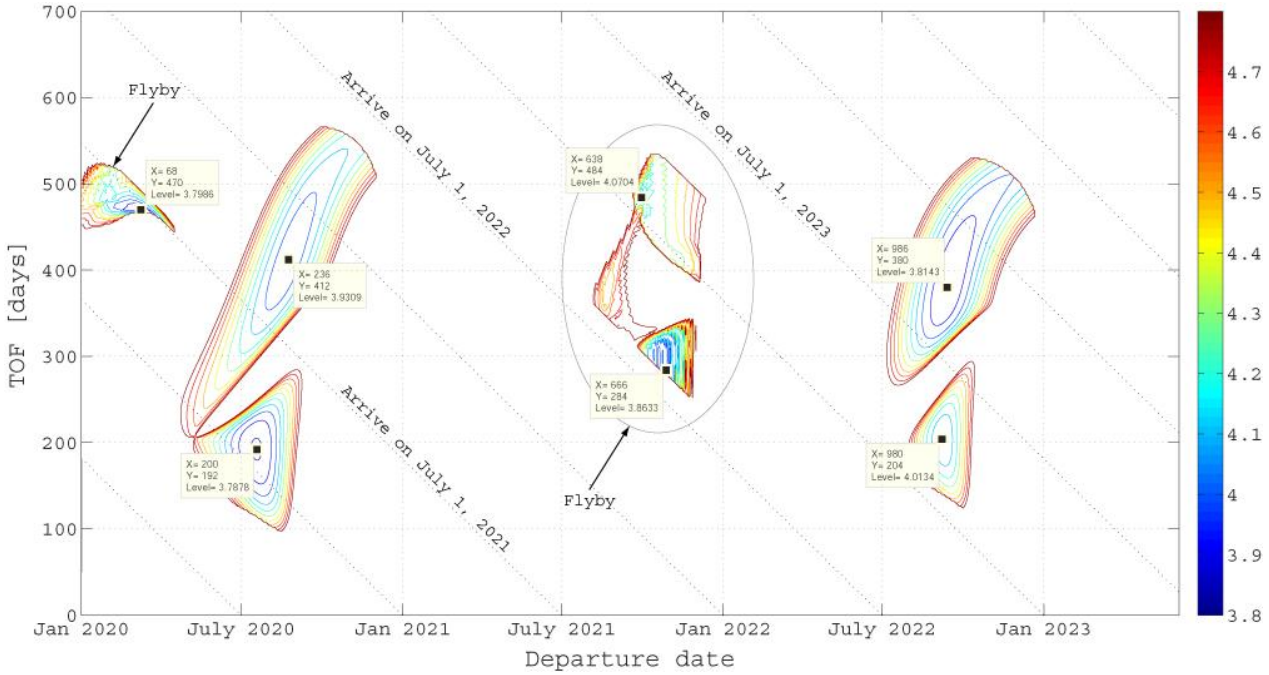

Fig. 9 Direct/flyby integrated ΔV_{tot} [km/s] contour plot: Earth-Mars/Earth-Venus-Mars.

4.2 Flight Opportunity Bat Chart

Fig. 10 shows an example of a single human Mars exploration mission scenario with all the launches comprising the transportation for the mission. This type of plot is referred to as a "bat chart" due to similarities in appearance to bats perching on a ceiling when showing elements upside down on the destination nodes at the top. In a time-expanded bat chart a mission scenario is indicated by edges, showing the movement of elements between nodes. As

in the example of the previous section, however, flight opportunities of interplanetary missions are highly time-dependent in terms of ΔV and thus possible edges in the bat chart are limited to some extent. Therefore, if all possible edges were drawn in a bat chart, it would be useful for finding a transportation schedule for future mission planning. Fig. 11 shows an example of this "flight opportunity bat chart", in which flight opportunities appear as a bunch of lines. This can be obtained from the ΔV_{tot} contour plot by scanning vertically for each departure date and filtering with some constraints on TOF, $C3_{\mathrm{d}}$, $C3_{\mathrm{a}}$, h_{m}, and ΔV_{PFM} (see below for how to define mission feasibility criteria). Blue lines represent direct flight opportunities and red lines represent flyby flight opportunities.

As seen above, a ΔV_{tot} contour plot and a flight opportunity bat chart can be used to see the flexibility of mission schedule and to perform a trade-off analysis between departure and arrival dates, TOF, $C3_{\mathrm{d}}$, $C3_{\mathrm{a}}$, and ΔV_{tot}, on a mission-by-mission basis.

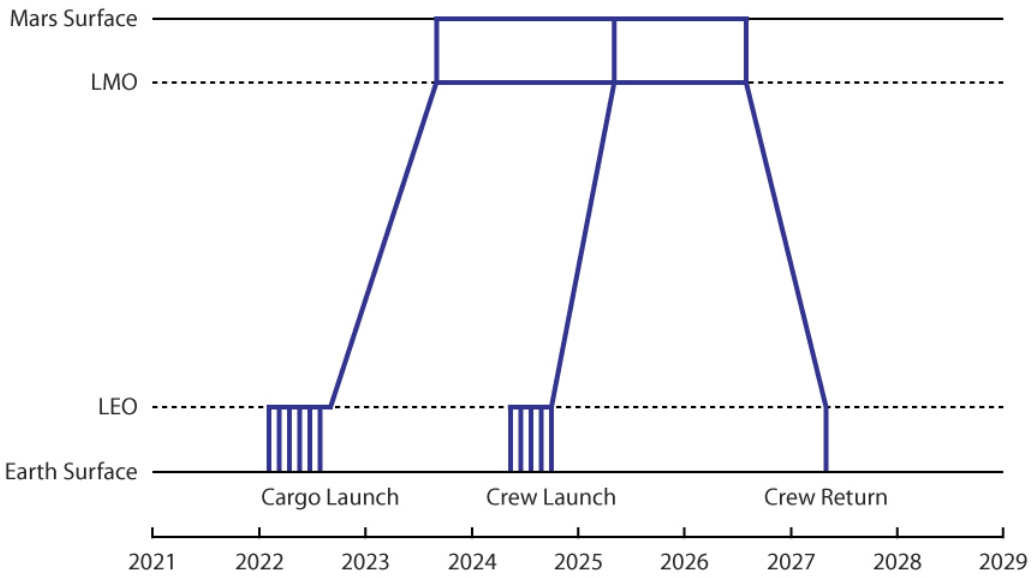

Fig. 10 Mars exploration bat chart illustrating campaign transports.

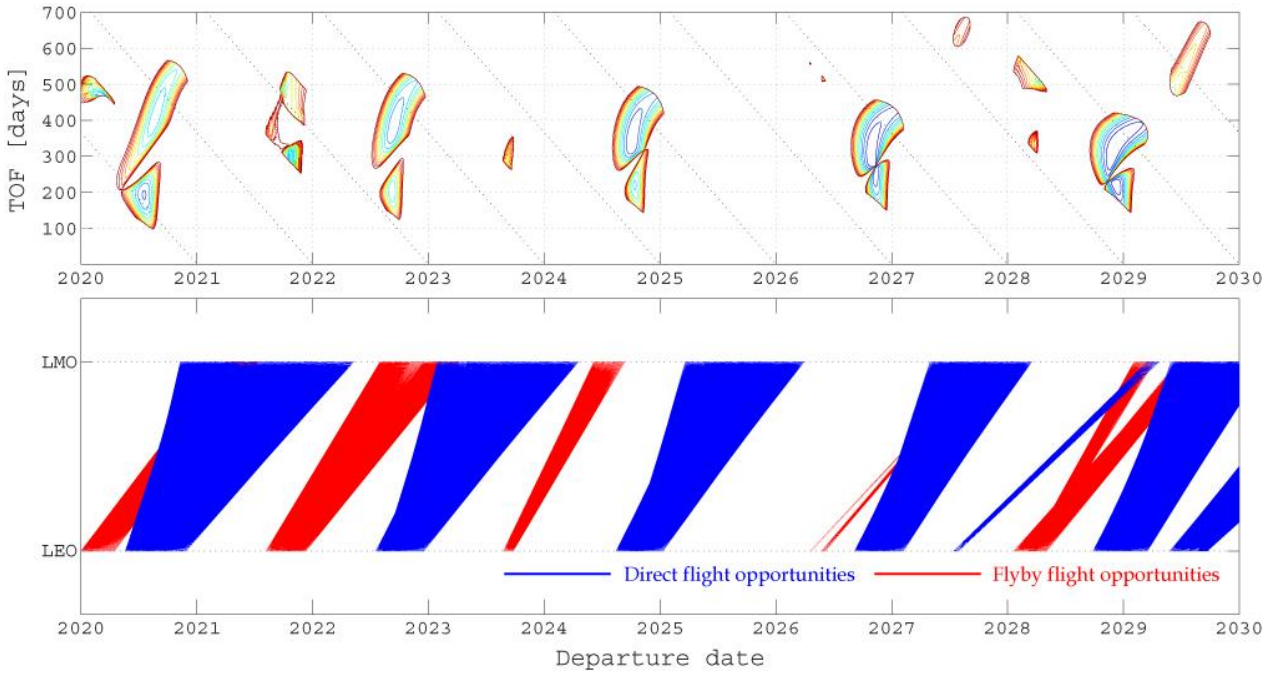

Fig. 11 Example of a "flight opportunity bat chart".

5. CASE STUDY: MARS MISSIONS INCLUDING VENUS FLYBYS

Mars missions including Venus flyby opportunities are analyzed in the time frame 2020 to 2040 and the competitiveness of Earth-Venus-Mars flyby trajectory windows with Earth-Mars direct trajectory windows is discussed.

5.1 Mission Feasibility Criteria

As the criteria for mission feasibility, the following four constraints are defined:

$C3_{\mathrm{d}}$: $C3_{\mathrm{d}}$ determines the launch feasibility. In a report from Jet Propulsion Laboratory, a feasible launch assumed that $C3_{\mathrm{d}}$ should be less than 25 [km^2/s^2] [7]. Considering envisioned advances in technology, a $C3_{\mathrm{d}}$ of 30 [km^2/s^2] was used as a launch feasibility criterion.

$C3_{\mathrm{a}}$: For direct entry or orbit insertion at arrival, propulsive capture generally requires lower arrival velocities, while aerocapture tolerates higher arrival velocities. Given an 8 [km/s] limit on Mars entry velocity, a $C3_{\mathrm{a}}$ at Mars up to 40 [km^2/s^2] is acceptable. On the other hand, from a previous analysis it is known that an Earth entry velocity up to 13 [km/s] is tolerable in terms of a deceleration g load and a heat load, which would rule out all trajectories with a $C3_{\mathrm{a}}$ at Earth over 45 [km^2/s^2] [10].

h_{m}: For flyby missions, considering the Venusian atmosphere, the flyby trajectory must pass well above the surface. It was assumed that a minimum passing altitude h_{m} of a feasible flight must be 250 km above the surface.

ΔV_{PFM}: Allowing a large amount of $|\Delta V_{\mathrm{PFM}}|$ would not make sense because it is originally desired to save fuel by taking advantage of the Venus gravitational field. In this study, 0.3 [km/s] was selected as a reasonable upper bound for $|\Delta V_{\mathrm{PFM}}|$.

$$C3_{\mathrm{d}} \leq 30 \text{ [km}^2\text{/s}^2\text{]} \tag{16}$$

$$C3_{\mathrm{a}} \leq 40 \text{ [km}^2\text{/s}^2\text{] (Mars arrival)} \tag{17}$$

$$C3_a \leq 45 \text{ [km}^2/\text{s}^2\text{] (Earth arrival)} \tag{18}$$

$$h_m \geq 250 \text{ [km]} \tag{19}$$

$$|\Delta V_{PFM}| \leq 0.3 \text{ [km/s]} \tag{20}$$

To save more time in the process of pseudo full-factorial computation in Fig. 8, since infeasible points with large $C3_d$ and $C3_a$ do not need to be calculated, they were screened out by the above constraints and a flyby calculation for such infeasible points was skipped. In the conversion from $C3_d$ to ΔV_d, a departure hyperbola starting from a circular parking orbit with an altitude of 300 km was assumed.

5.2 Simulation Results and Discussions

Fig. 12 shows a direct/flyby integrated ΔV_{tot} contour plot for 2020-2040 Earth-Mars trajectories. The required computation time to produce this contour plot was about 70 hours for direct trajectories plus 140 hours for flyby trajectories (MATLAB® used on Intel® Core™2 Duo processor at 2.40 GHz). This contour plot displays ΔV_{tot} up to 4.8 [km/s]. Note that the contours were filtered by the constraints for $C3_d$, $C3_a$, h_m, and ΔV_{PFM} in Eqs. (16) through (20). Therefore, the "craters" in the figure mean feasible regions in terms of the above criteria. The local minimum ΔV_{tot} in each crater is listed in Table 1 as a representative of the launch opportunity. The "competitiveness" of each opportunity is determined by the following criteria: (1) if two neighbor opportunities have an overlapping departure date (an overlapping arrival date), and one has an earlier arrival date (a later departure date) than the other, the other is regarded as "dominated" since a shorter TOF would be desirable from the perspective of exposure to both reduced gravity and space radiation, or (2) if an opportunity does not have neighbors with overlapping departure or arrival dates, the opportunity is non-dominated and thus regarded as "competitive" since it would add a new launch window even if it requires a relatively high ΔV_{tot} [11]. As a result, six out of seven flyby windows are competitive. Earth-Venus-Mars flyby trajectories tend to have a relatively high ΔV_{tot} but give new opportunities. Having more launch windows available provides flexibility of mission planning.

Fig. 13 shows a direct/flyby integrated ΔV_{tot} contour plot for 2020-2040 Mars-Earth return trajectories. This contour plot displays ΔV_{tot} up to 4.2 [km/s]. The local minimum ΔV_{tot} in each crater is listed in Table 2 as a representative of the launch opportunity. As a result, all the four flyby windows are competitive. Mars-Venus-Earth flyby trajectories have a much higher ΔV_{tot} and a longer TOF but make more launch windows available. In general, Mars-Venus-Earth flyby trajectories are said to be inefficient since a spacecraft first heads for Venus, an inferior planet, which would require higher energy for departure than a direct trip to Earth. However, it is interesting that all the flyby windows are found to be "competitive" and thus significant since they open up additional opportunities that cannot be replaced by the direct flight opportunities.

Figs. 14 and 15 show 2020-2040 Earth-Mars and Mars-Earth flight opportunity bat charts, respectively. A set of lines between the nodes "LEO" (low Earth orbit) and "LMO" (low Mars orbit) can be seen in the figures, each of which connects departure node and date as a feasible combination.

6. CONCLUSIONS

This paper develops a tool which is capable of solving Lambert's problem to calculate ballistic interplanetary trajectories and formulates a method to create an exhaustive ΔV_{tot} contour plot for both direct and flyby trajectories in a single chart. While a full-factorial computation is used for the direct trajectory case, a "pseudo full-factorial" approach proposed in this paper enables to visualize the flyby windows in a reasonable amount of effort. Subsequently, a "flight opportunity bat chart" is also drawn. Both a ΔV_{tot} contour plot and a flight opportunity bat chart would serve as a "visual calendar" of launch windows, which is a useful database for the creation of a long-term transportation schedule for mission planning purposes.

Mars missions including Venus flyby opportunities in the time frame 2020-2040 are used to illustrate the application of the methods and charts developed in this work. Earth-Mars/Earth-Venus-Mars and Mars-Earth/Mars-Venus-Earth integrated ΔV_{tot} contour plots, trajectory data tables, and flight opportunity bat charts are obtained. It is found that almost all of the Venus flyby opportunities are of significance since they give additional launch windows that cannot be covered by the direct flight windows. Venus flyby trajectories can be even more important if a permanent presence is established on Mars because they can be additional re-supply windows.

REFERENCES

1. Review of U.S. Human Spaceflight Plans Committee, "Seeking A Human Spaceflight Program Worthy of A Great Nation", Washington, D.C., October 2009.
2. C. Bolden, "Statement by Charlie Bolden", NASA Budget Press Conference, February 2010.
3. B. Obama, "Remarks by the President on Space Exploration in the 21st Century", April 2010.
4. T. Ishimatsu, "Interplanetary Trajectory Analysis for 2020-2040 Mars Missions including Venus Flyby Opportunities", Master's Thesis, Massachusetts Institute of Technology, May 2008.
5. T. Ishimatsu, J. Hoffman, and O. de Weck, "Interplanetary Trajectory Analysis for 2020-2040 Mars Missions including Venus Flyby Opportunities", AIAA 2009-6470, SPACE 2009, Pasadena, CA, September 2009.
6. T. Ishimatsu, P. Grogan, and O. de Weck, "Interplanetary Trajectory Analysis and Logistical Considerations of Human Mars Exploration", *Journal of Cosmology*, Vol. 12, 3588-3600, October 2010.
7. S. Matousek and A. Sergeyevsky, "To Mars and Back: 2002-2020 Ballistic Trajectory Data for the Mission Architect", AIAA 98-4396, AIAA/AAS Astrodynamics Specialist Conference, Boston, MA, August 1998.
8. R. Battin, "*An Introduction to the Mathematics and Methods of Astrodynamics, Revised Edition*", AIAA Education Series, 1999.
9. R. Bate, D. Mueller, and J. White, "*Fundamentals of Astrodynamics*", Dover Publications, 1971.
10. E. Crawley, et al., "Draper/MIT Concept Exploration and Refinement (CE&R) Study – Final Report", September 2005.
11. G. Walberg, "How Shall We Go to Mars? A Review of Mission Scenarios", *Journal of Spacecraft and Rockets*, Vol. 30, No. 2, 1993, pp. 129-139.

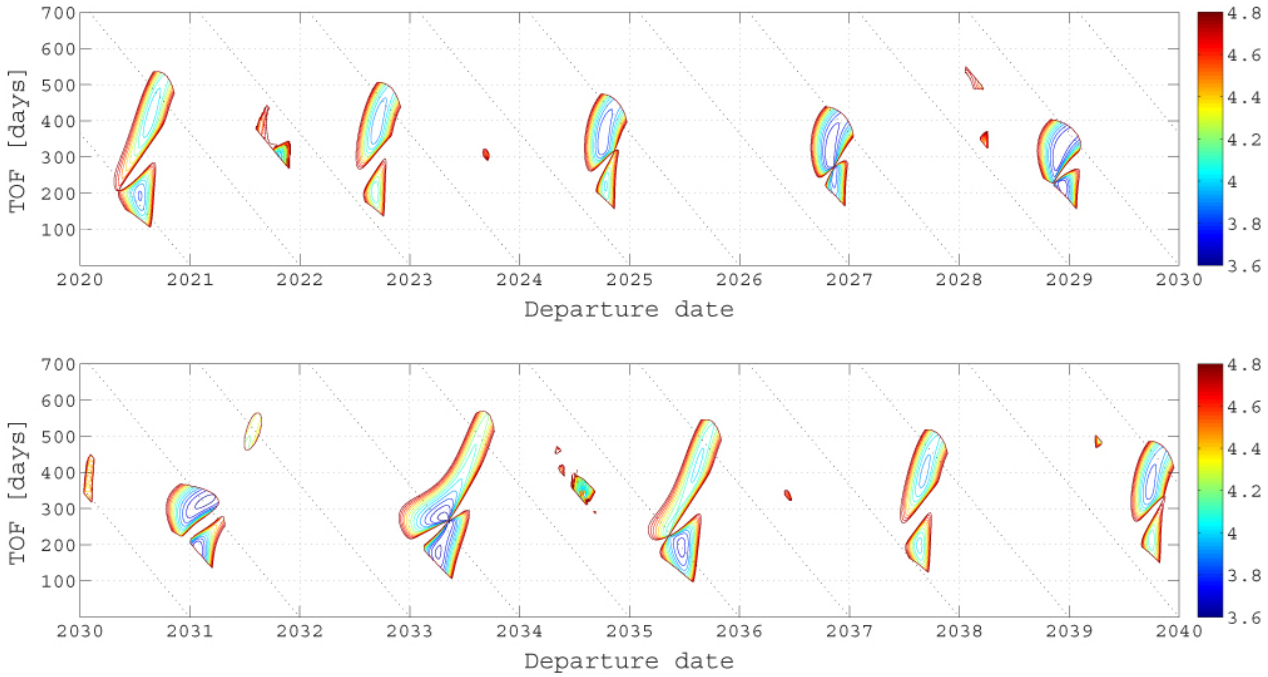

Fig. 12 2020-2040 Earth-Mars ΔV_{tot} [km/s] contour plot.

TABLE 1: *2020-2040 Earth-Mars Trajectory Data.*

						departure	dep. (+ flyby)	arrival	
#	Trajectory	Departure	Flyby	Arrival	TOF [days]	C3d [km^2/s^2]	ΔVtot [km/s]	C3a [km^2/s^2]	Competitiveness
1	2020 Earth-Mars	07/17/20	-	01/27/21	194	13.20	3.788	8.19	competitive
2	2020 Earth-Mars	08/24/20	-	10/10/21	412	16.50	3.931	14.52	dominated
3	2021 Earth-Venus-Mars	11/01/21	03/27/22	08/28/22	300 (= 146 + 154)	14.32	3.873	33.60	competitive
4	2022 Earth-Mars	09/07/22	-	03/30/23	204	18.43	4.013	13.51	competitive
5	2022 Earth-Mars	09/15/22	-	10/04/23	384	13.79	3.814	9.59	dominated
6	2023 Earth-Venus-Mars	09/14/23	02/19/24	07/16/24	306 (= 158 + 148)	26.02	4.363	39.80	competitive
7	2024 Earth-Mars	10/04/24	-	09/13/25	344	11.19	3.701	6.39	dominated
8	2024 Earth-Mars	10/12/24	-	05/20/25	220	17.73	3.984	17.02	competitive
9	2026 Earth-Mars	10/30/26	-	08/20/27	294	9.14	3.611	7.32	dominated
10	2026 Earth-Mars	11/13/26	-	08/10/27	270	10.88	3.687	8.40	competitive
11	2028 Earth-Venus-Mars	03/19/28	08/20/28	02/22/29	340 (= 154 + 186)	26.80	4.377	39.68	competitive
12	2028 Earth-Mars	12/02/28	-	10/18/29	320	8.93	3.601	10.97	dominated
13	2028 Earth-Mars	12/10/28	-	07/20/29	222	9.05	3.607	23.71	competitive
14	2030 Earth-Venus-Mars	01/28/30	07/11/30	01/23/31	362 (= 166 + 196)	25.00	4.297	24.57	competitive
15	2031 Earth-Mars	01/27/31	-	08/05/31	190	9.00	3.605	31.05	competitive
16	2031 Earth-Mars	02/22/31	-	01/08/32	320	8.24	3.571	30.48	dominated
17	2031 Earth-Mars	07/04/31	-	10/10/32	464	21.62	4.149	39.99	competitive
18	2033 Earth-Mars	04/06/33	-	10/01/33	178	8.42	3.579	15.49	competitive
19	2033 Earth-Mars	04/28/33	-	01/27/34	274	7.78	3.551	19.16	dominated
20	2034 Earth-Venus-Mars	07/26/34	12/09/34	07/15/35	354 (= 136 + 218)	14.25	3.836	31.16	competitive
21	2035 Earth-Mars	06/23/35	-	01/05/36	196	10.20	3.657	7.22	competitive
22	2035 Earth-Mars	08/14/35	-	10/03/36	416	17.52	3.975	16.73	dominated
23	2036 Earth-Venus-Mars	06/11/36	11/22/36	05/11/37	334 (= 164 + 170)	24.26	4.421	39.85	competitive
24	2037 Earth-Mars	08/21/37	-	03/07/38	198	17.07	3.955	11.29	competitive
25	2037 Earth-Mars	09/06/37	-	10/07/38	396	14.85	3.860	11.22	dominated
26	2039 Earth-Venus-Mars	04/19/39	08/25/39	08/15/40	484 (= 128 + 356)	20.09	4.099	39.79	dominated
27	2039 Earth-Mars	09/28/39	-	09/24/40	362	12.18	3.744	7.46	dominated
28	2039 Earth-Mars	09/30/39	-	05/01/40	214	18.66	4.023	16.09	competitive

***Flyby missions are shaded.**

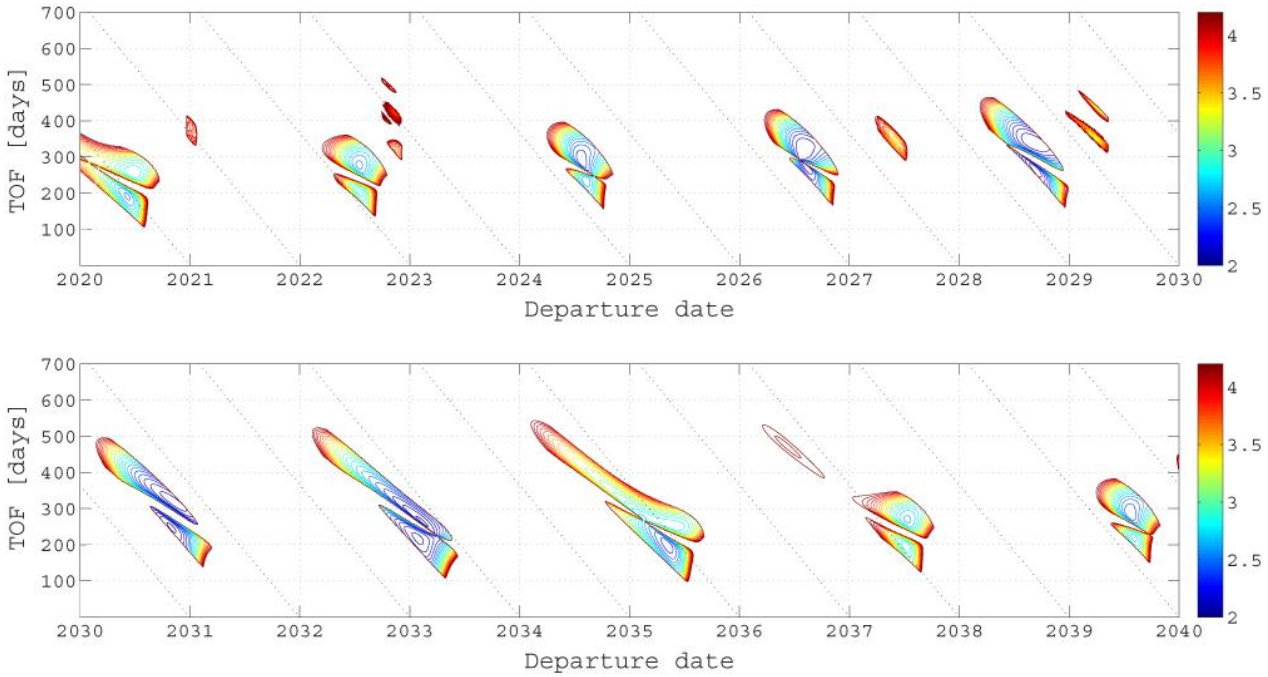

Fig. 13 2020-2040 Mars-Earth ΔV_{tot} [km/s] contour plot.

TABLE 2: *2020-2040 Mars-Earth Trajectory Data.*

#	Trajectory	Departure	Flyby	Arrival	TOF [days]	departure C3d [km^2/s^2]	dep. (+ flyby) ΔVtot [km/s]	arrival C3a [km^2/s^2]	Competitiveness
1	2020 Mars-Earth	06/05/20	-	12/14/20	192	11.44	2.480	10.93	competitive
2	2020 Mars-Earth	06/25/20	-	03/10/21	258	14.11	2.702	17.42	dominated
3	2021 Mars-Venus-Earth	01/07/21	08/07/21	01/26/22	384 (= 212 + 172)	27.64	3.726	17.81	competitive
4	2022 Mars-Earth	07/17/22	-	04/19/23	276	11.36	2.473	10.09	dominated
5	2022 Mars-Earth	07/21/22	-	02/10/23	204	14.76	2.755	17.42	competitive
6	2021 Mars-Venus-Earth	11/02/22	07/14/23	01/02/24	426 (= 254 + 172)	24.33	3.491	27.31	competitive
7	2024 Mars-Earth	07/24/24	-	05/10/25	290	8.61	2.234	7.90	dominated
8	2024 Mars-Earth	08/09/24	-	03/31/25	234	12.02	2.529	18.76	competitive
9	2026 Mars-Earth	08/03/26	-	06/19/27	320	7.17	2.104	9.48	dominated
10	2026 Mars-Earth	08/11/26	-	05/12/27	274	7.28	2.114	19.19	competitive
11	2027 Mars-Venus-Earth	06/07/27	12/06/27	05/18/28	346 (= 182 + 164)	22.81	3.377	24.18	competitive
12	2028 Mars-Earth	09/05/28	-	08/11/29	340	6.15	2.012	19.88	dominated
13	2028 Mars-Earth	09/11/28	-	06/02/29	264	6.46	2.040	31.85	competitive
14	2029 Mars-Venus-Earth	04/01/29	10/20/29	03/19/30	352 (= 202 + 150)	19.23	3.109	36.81	competitive
15	2030 Mars-Earth	10/31/30	-	07/06/31	248	5.79	1.978	32.30	competitive
16	2030 Mars-Earth	11/10/30	-	09/24/31	318	5.43	1.945	30.34	dominated
17	2033 Mars-Earth	01/28/33	-	09/03/33	218	5.72	1.971	16.10	competitive
18	2033 Mars-Earth	02/11/33	-	11/02/33	264	5.81	1.980	24.33	dominated
19	2035 Mars-Earth	02/17/35	-	11/12/35	268	12.90	2.602	9.79	dominated
20	2035 Mars-Earth	05/08/35	-	11/22/35	198	8.77	2.248	9.18	competitive
21	2037 Mars-Earth	07/08/37	-	01/20/38	196	14.31	2.719	14.94	competitive
22	2037 Mars-Earth	07/12/37	-	04/08/38	270	12.55	2.573	12.54	dominated
23	2039 Mars-Earth	07/22/39	-	05/03/40	286	9.59	2.320	8.13	dominated
24	2039 Mars-Earth	08/05/39	-	03/12/40	220	13.60	2.661	19.15	competitive

*Flyby missions are shaded.

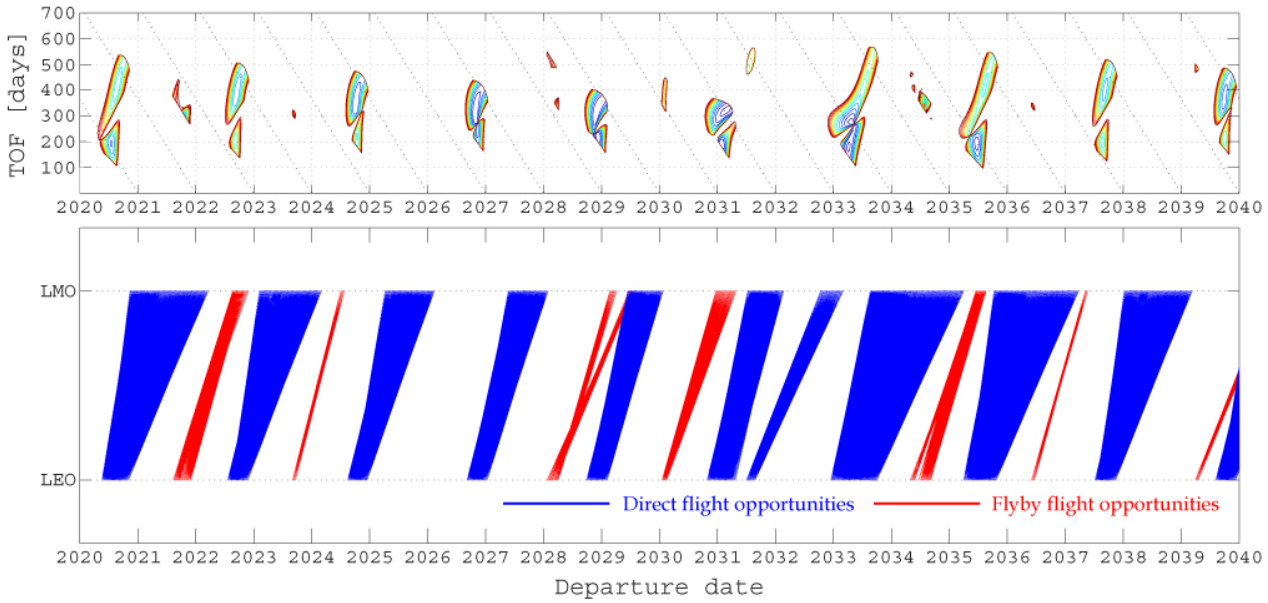

Fig. 14 2020-2040 Earth-Mars flight opportunity bat chart.

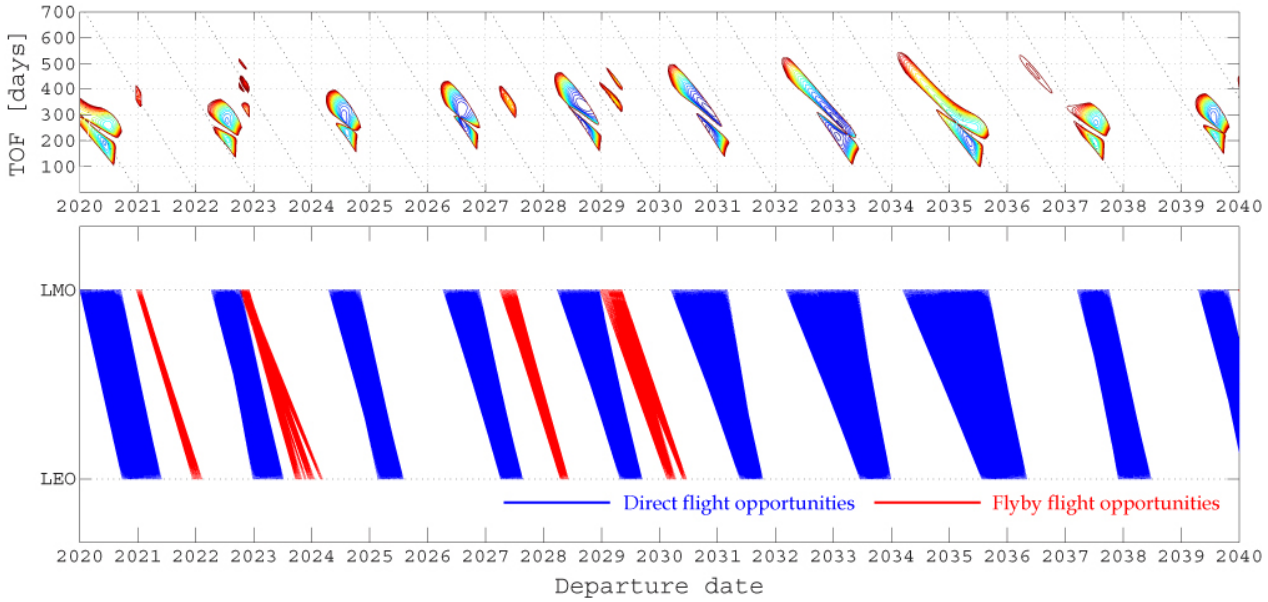

Fig. 15 2020-2040 Mars-Earth flight opportunity bat chart.